Cymer Inc., ASML, TRW, Xtreme Technologies GmbH, Fraunhoffer Institut fur Lasertechnik, Philips Extreme UV GmbH, Royal Institute of Technology Sweden, PLEX LLC.

Disco Corporation, http://www.disco.co.jp/

Exitech Ltd., http://www.exitech.co.uk/

Lamda Physik, http://www.lambdaphysik.de/

Meyer KA, Besemann DM and Wright JC (2003) Coherent two dimensional spectroscopy with triply vibrationally enhanced infrared four-wave mixing. *Chemical Physics Letters* 381: 642–649.

Perkin Elmer, www.perkinelmer.com

Phillips D (1997) Chemical mechanisms in photodynamic therapy with phthalocyanines. *Progress in Reaction Kinetics* 22(3–4): 175–300.

Potma EO and Xie X-S (2003) Detection of single lipid bilayers with coherent anti-Stokes Raman scattering (CARS) microscopy. *Journal of Raman Spectroscopy* 34: 642–650.

Powerlase Ltd., http://www.powerlase.com

Presstek Inc., Hudson, NH, http://www.presstek.com

Pronko PP, Dutta DK, Squier J, Rudd JV, Du D and Mourou G (1995) Machining of sub-micron holes using a femtosecond laser at 800 nm. *Optics Communications* 114: 106–110.

Reiser A (1989) *Photoreactive Polymers – The Science and Technology of Resists*. John Wiley & Sons.

Silverman PJ (2002) Intel Corporation. Presented at 1st Intl EUV Lithography Symposium, 15–17 October 2002, Dallas, USA.

Stuart BC, Feit MD, Herman S, Rubenchik AM, Shore BW and Perry MD (1996) Nanosecond-to-femtosecond laser-induced breakdown in dielectrics. *Physics Review B* 53(4): 1749.

Svanberg S (1996) Chemical sensing with laser spectroscopy. *Sensors and Actuators B* 33: 1–4.

Wang I, Bendsoe N, Klinteberg CAF, *et al*. (2001) Photodynamic therapy vs. cryosurgery of basal cell carcinomas: results of a phase III clinical trial. *British Journal of Dermatology* 144(4): 832–840.

Watson MN (1984) Laser drilling of printed circuit boards. *Circuit World* 11: 13.

Waynant RW (ed.) (2002) *Lasers in Medicine*. CRC Press.

Weibring P, Edner H and Svanberg S (2003) Versatile mobile lidar system for environmental monitoring. *Applied Optics* 42(18): 3583–3594.

WITEC, WITec Wissenschaftliche, Instrumente und Technologie GmbH, Hörvelsinger Weg 6, D-89081 Ulm, Germany, www.WITec.de

Yvon J, www.jobinyvon.com

Sum-Frequency Generation at Surfaces

M B Raschke and Y R Shen, University of California, Berkeley, CA, USA

Introduction

Under sufficiently intense illumination the optical properties of a material system depend nonlinearly on the strength of the electromagnetic field. Related to this nonlinear optical response is a large number of phenomena and fundamental processes which are discussed in various articles of this encyclopedia. This article will focus on second-harmonic generation (SHG) and sum-frequency generation (SFG) for the investigation of surfaces and interfaces. The intrinsic surface sensitivity of these techniques allows for investigations of surface properties not readily accessible by other spectroscopies. Here, the basic principles of these optical processes as well as their experimental implementation are discussed, and a summary of the applications to different material systems is given.

Among the various techniques employed for the characterization of surfaces and interfaces, those using light are particularly attractive. They are applicable *in situ* to all interfaces accessible by light, are nondestructive, and offer unprecedented time resolution. However, the penetration depth of optical radiation in matter is generally of the order of a wavelength, which makes isolation of the surface or interface contribution to the optical response from the bulk contribution difficult. In contrast, for reasons of symmetry, SHG and SFG are intrinsically surface sensitive in media with inversion symmetry, and hence the signal generated mainly originates from the topmost surface layer where the inversion symmetry is broken. By means of electronic or vibrational SHG or SFG spectroscopy, information on surface structure, chemical composition and bond or molecular orientation at solid and liquid interfaces can be deduced. To date, SFG and SHG have been well established as important tools for the investigation of surfaces and interfaces of solids ranging from metals and semiconductors to insulators and magnetic materials, liquids, polymers, biological membranes, and other systems. The studies are motivated by fundamental interests as well as applications in many areas such as heterogeneous catalysis, electrochemistry, device fabrication, epitaxial growth, and environmental science.

Theory

The nonlinear optical response of a material, in the electric-dipole approximation, can often be described by an induced polarization in the form of a power series,

$$\begin{aligned}\boldsymbol{P}(\omega) = \epsilon_0[&\chi^{(1)}(\omega)\boldsymbol{E}(\omega) \\ &+\chi^{(2)}(\omega=\omega_1+\omega_2)\boldsymbol{E}(\omega_1)\boldsymbol{E}(\omega_2) \\ &+\chi^{(3)}(\omega=\omega_1+\omega_2+\omega_3)\boldsymbol{E}(\omega_1)\boldsymbol{E}(\omega_2)\boldsymbol{E}(\omega_3)+\ldots]\end{aligned} \quad [1]$$

where $\boldsymbol{E}(\omega_i)$ is the optical field with frequency ω_i and $\chi^{(n)}$ is the nth-order linear ($n=1$) or nonlinear ($n>1$) susceptibility tensor. The second term, being the lowest-order nonlinear optical response, is responsible for sum-frequency generation and second-harmonic generation (with $\omega_1=\omega_2$). In the electric-dipole approximation, all even-order terms ($\chi^2, \chi^{(4)}$, etc.) are forbidden in media with inversion symmetry. At the surface or interface, however, the inversion symmetry is necessarily broken and hence $\chi^{(2)} \neq 0$. This makes SHG and SFG surface-sensitive and specific. While electric-quadrupole and magnetic-dipole contributions from the bulk may not be totally negligible, in many cases it has been shown that the surface contribution clearly dominates.

Surface SFG and SHG is best described by radiation from a surface polarization $\boldsymbol{P}_s^{(2)}(\omega)$ induced in a thin sheet with dielectric constant ε' sandwiched between two linear media (1) and (2) as shown schematically in Figure 1. This surface polarization has an in-plane wavevector component equal to the sum of the in-plane wavevector components of the incident fields:

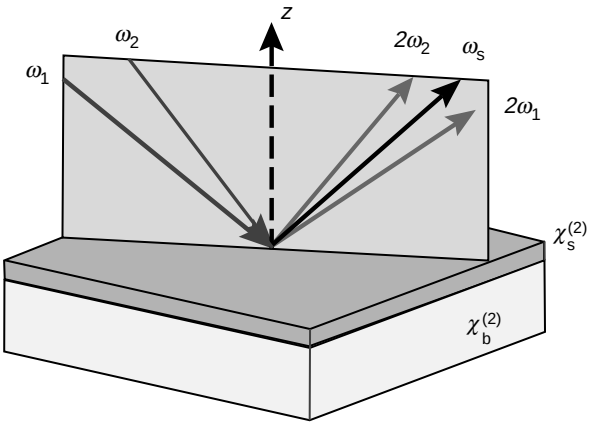

Figure 1 Schematic of SHG and SFG geometry in reflection and transmission from an interface.

$\boldsymbol{k}_\parallel(\omega) = \boldsymbol{k}_\parallel(\omega_1) + \boldsymbol{k}_\parallel(\omega_2)$. The ratio of $\boldsymbol{k}_\parallel(\omega)$ to $\boldsymbol{k}(\omega)$ then determines the direction of the sum-frequency output that appears in both transmission and reflection. The reflection geometry is often used in order to minimize the bulk contribution.

With $\boldsymbol{P}_s^{(2)}$ as the source term, the sum-frequency output can be obtained from the solution of the wave equation. With the proper boundary conditions the sum frequency (SF) intensity is given by:

$$\begin{aligned}I(\omega) = &\frac{8\pi^3\omega_s^2\sec^2\theta_\omega}{\hbar c^3\sqrt{\epsilon_1(\omega)\epsilon_1(\omega_1)\epsilon_1(\omega_2)}} \\ &\times |\boldsymbol{e}^\dagger(\omega)\cdot\boldsymbol{\chi}_s^{(2)} : \boldsymbol{e}(\omega_1)\boldsymbol{e}(\omega_2)|^2 I_1(\omega_1)I_2(\omega_2)\end{aligned} \quad [2]$$

In this expression, $\chi_s^{(2)}$ is the surface nonlinear susceptibility defined by $\boldsymbol{P}_s^{(2)} = \varepsilon_0\boldsymbol{\chi}_s^{(2)} : \boldsymbol{E}(\omega_1)\boldsymbol{E}(\omega_2)$; the quantities $\boldsymbol{e}(\omega_i)$ correspond to the unit polarization vectors after the appropriate Fresnel correction, $\boldsymbol{e}(\omega_i) \equiv \boldsymbol{F}(\omega_i)\hat{\boldsymbol{e}}(\omega_i)$, with $\boldsymbol{F}(\omega_i)$ being the transmission Fresnel factor and $\hat{\boldsymbol{e}}(\omega_i)$ the unit polarization vector of $\boldsymbol{E}(\omega_i)$; θ_ω denotes the SF output angle with respect to the surface normal, $\varepsilon(\omega_i)$ is the dielectric constant at frequency ω_i, and I_i is the input pump intensity at ω_i.

The surface nonlinear susceptibility $\chi_s^{(2)}$ is a third-rank tensor. In Cartesian coordinates it has 27 tensor elements ($\chi_{ijk}^{(2)}$), many of which could vanish or depend on others due to the surface structural symmetry. As an example, $\chi_{ijk}^{(2)}(\omega=\omega_1+\omega_2)$ for an isotropic surface, with the z-direction defined by the surface normal, has only four independent nonvanishing elements: $\chi_{xxz}^{(2)} = \chi_{yyz}^{(2)}, \chi_{xzx}^{(2)} = \chi_{yzy}^{(2)}, \chi_{zxx}^{(2)} = \chi_{zyy}^{(2)}$, and $\chi_{zzz}^{(2)}$. Different combinations of input and output beam polarizations in SFG measurements are often used to deduce values for the non-vanishing elements. Such measurements then allow the determination of surface symmetry or surface molecular orientation. Being a third-rank tensor, $\chi_s^{(2)}$ can reflect up to three-fold rotational symmetry. $\chi_{s,ijk}^{(2)}$ is related to the molecular nonlinear polarizability or hyperpolarizability $\alpha_{\xi\eta\zeta}^{(2)}$, where $\hat{\xi}$, $\hat{\eta}$, and $\hat{\zeta}$ define the molecular coordinates, through the coordinate transformation

$$\chi_{s,ijk}^{(2)} = N_s\left\langle(\hat{\boldsymbol{i}}\cdot\hat{\boldsymbol{\xi}})(\hat{\boldsymbol{j}}\cdot\hat{\boldsymbol{\eta}})(\hat{\boldsymbol{k}}\cdot\hat{\boldsymbol{\xi}})\right\rangle\alpha_{\xi\eta\zeta}^{(2)} \quad [3]$$

The angular brackets denote an average over the molecular orientational distribution, and N_s is the surface molecular density. For simplicity, microscopic local-field correction is neglected in eqn [3]. Knowing $\chi_{s,ijk}^{(2)}$ and $\alpha_{\xi\eta\zeta}^{(2)}$ thus permits deduction of information on the orientational distribution.

An explicit expression for the nonlinear optical polarizability is obtained from a second-order quantum mechanical perturbation calculation:

$$\alpha^{(2)}_{s,ijk}(\omega_s) = -\frac{e^3}{\hbar^2}\sum_{g,n,n'}\left[\frac{\langle g|r_i|n\rangle}{\omega_s-\omega_{ng}+i\Gamma_{ng}} \times\left(\frac{\langle n|r_j|n'\rangle\langle n'|r_k|g\rangle}{\omega_2-\omega_{n'g}+i\Gamma_{n'g}} + \frac{\langle n|r_k|n'\rangle\langle n'|r_j|g\rangle}{\omega_1-\omega_{n'g}+i\Gamma_{n'g}}\right)+\cdots\right]\rho^{(0)}_g \quad [4]$$

This expression shows how the nonlinear polarizability or susceptibility depends on material parameters such as the dipole transition moments $\langle n|r_i|g\rangle$ and energy levels. It contains a sum over eight resonant terms. The quantities ω_{ng} and Γ_{ng} are the frequencies and half-widths for the transitions between quantum states $|n\rangle$ and $|g\rangle$, and $\rho^{(0)}_g$ denotes the population in $|g\rangle$. It can be seen that $\alpha^{(2)}$, and hence the SF output, should be resonantly enhanced when the pump frequency ω_1 or ω_2 and/or the sum frequency $\omega_1+\omega_2$ approach resonance. The resonant enhancement provides spectral information and makes SHG and SFG effective spectroscopic tools. The resonances could be electronic or vibrational, or more generally, any surface characteristic transition.

Experimental

Here we deal with basic considerations concerning the optical setup for SHG or SFG experiments in reflection from a surface as is shown schematically in Figure 2. In general, the pump radiation from pulsed laser sources is directed onto the surface. High-power tunable light pulses can be obtained from optical parametric generation and amplification (OPG/OPA) together with harmonic, sum- or difference-frequency generation, preferably pumped by picosecond or femtosecond lasers with high repetition rates. By this means radiation tunable from near UV at ~200 nm to mid IR at ~18 μm can be generated. For SFG the input pulses with frequencies ω_1 and ω_2 are directed to overlap spatially and temporally on the sample. The sample could be the surface of a liquid or solid in air, a single crystalline surface in ultrahigh vacuum, buried interfaces, etc. Polarizers and half-wave plates allow for tuning of incident power and polarizations at the sample. Together with the polarizer in the output path, different input/output polarization combinations can be chosen. In the detection system the signal has to be discriminated against reflected and scattered pump light. This is achieved by spatial and spectral filtering with apertures, dielectric mirrors, and interference and color glass filters. An optional monochromator can also be used for additional stray-light suppression. The signal is then detected by a photomultiplier tube and gated electronics are used for signal integration or photon counting.

From eqn [2] the expected signal strength for SHG/SFG can be estimated. With a typical value of $\chi^{(2)}_s$ of 10^{-21} m^2 V^{-1}, a single 1-μm pump pulse, incident at $\theta = 45°$ having pulse energy $E = I\,A\tau = 100$ μJ, beam cross-section $A = 1$ mm^2, and pulse duration $\tau = 10$ ps, can generate about 10^3 photons per pulse of SHG. By means of photon counting a minimal count rate of 10^{-3} photons/pulse

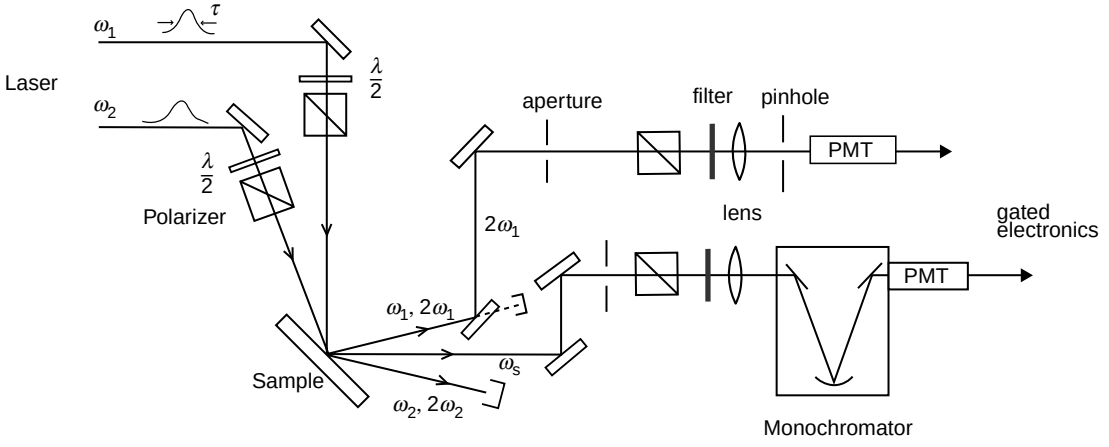

Figure 2 Schematic of experimental setup for second-harmonic and sum-frequency generation.

can be achieved which allows the detection of $\chi_s^{(2)}$ as small as 10^{-24} $m^2\,V^{-1}$. The spectral resolution is limited by the spectral width of the pump pulses. In order to obtain accurate spectral data over a wide tuning range or to obtain absolute values for $\chi_{s,ijk}^{(2)}$ of the material investigated, a reference material such as *z*-cut quartz with known values of χ is to be measured for comparison.

The simplest kind of experiments are SHG at a fixed pump frequency. From the signal variation in response to surface modification one can probe kinetics and dynamics of adsorption, desorption, diffusion, surface melting, phase transitions, etc. By tuning the pump wavelength, second-harmonic spectroscopy can give information on surface electronic states. For surface vibrational spectroscopy, however, IR-vis SFG must be employed. In the latter case, tunable IR input is mixed with visible input to yield a SF signal in the visible region.

Surface Specificity

In many cases, the surface contribution to SFG or SHG from a centrosymmetric medium clearly dominates over the bulk contribution. This generally occurs when the surface or interface is composed of a polar oriented molecular layer. An example is shown in Figure 3, where the vibrational spectra in the C–H stretch region of three buried solid–liquid interfaces are presented. The spectrum for hexadecane ($C_{16}H_{34}$)/fused silica shows no C–H peaks. This is in spite of the fact that liquid hexadecane has strong infrared and Raman activity in this spectral range. The result indicates that the bulk signal contribution is negligible. In contrast, strong resonances are observed from the hexadecane/OTS/silica system, where OTS is a monolayer of octadecyltrichlorosilane ($CH_3(CH_2)_{17}SiCl_3$) chemisorbed on the fused silica plate. A similar spectrum is obtained for the CCl_4/OTS/silica interface. This clearly indicates that it is the contribution from the OTS monolayer that dominates the spectra.

Another example is described in Figure 4 where the SFG spectrum in reflection from a free liquid water surface is shown. The resonant features between 3000 and 3600 cm^{-1} are due to the O–H stretches of hydrogen-bonded OH groups. The sharp peak at 3700 cm^{-1} can be identified with the free OH bonds. Since no dangling OH bonds can exist below the surface its presence indicates that the spectrum must originate from the topmost layer of water molecules. Furthermore it can be shown that the surface water molecules are oriented with one of the OH bonds directed out of the liquid. In addition to the above examples, the surface sensitivity and specificity has been demonstrated and successfully applied to a large number of systems as will be shown below.

A note on the definition of surface or interface is in order. In SHG and SFG, the surface or interface layer refers to a thin layer between two adjacent bulk media that has a different structure from the bulk media and lacks inversion symmetry. If molecules in the surface layer are polar-ordered, then SHG and

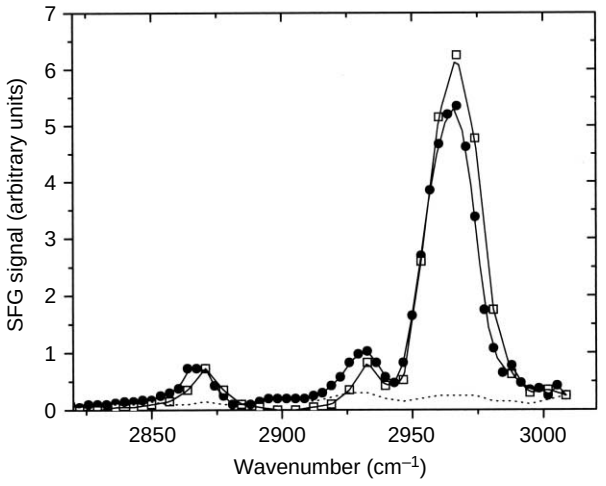

Figure 3 SFG spectra of different interfaces obtained with *ssp* polarization combination: hexadecane/silica (dashed), CCl_4/ OTS/silica (solid circles), and hexadecane/OTS/silica (open squares). OTS refers to a monolayer of octadecyltrichlorosilane.

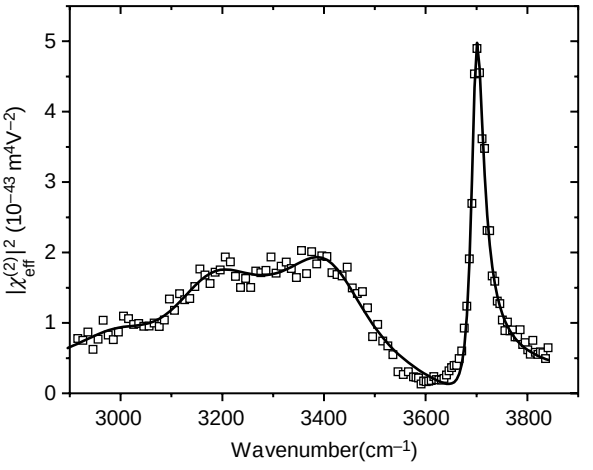

Figure 4 SFG spectrum of the liquid–vapor interface of pure water (*ssp* polarization combination). The mode at 3700 cm^{-1} is due to the dangling OH bonds at the surface.

SFG are often dominated by contributions from the surface layer. However, the bulk contribution is not strictly zero even if the media have inversion symmetry, as $\chi^{(2)}$ can arise from electric-quadrupole and magnetic-dipole contributions. Separation of surface and bulk contributions in SHG and SFG is a subtle problem in general. Experimentally, how surface modification affects the signal can be used to evaluate whether or not the surface contribution dominates.

A special case concerns materials that lack bulk inversion symmetry, for example, III–V and II–VI semiconductors such as GaAs and ZnSe. In this case, the bulk contribution to SHG and SFG is electric-dipole allowed and may be very significant. With an appropriate choice of polarization combinations and surface orientation, it can nevertheless be well suppressed, leaving the surface contribution dominant.

Applications

Both SFG and SHG have been applied to a wide variety of surface and interfacial systems. To illustrate their capabilities and versatility as surface spectroscopic tools, the focus of this summary will be on examples where the information deduced cannot readily be obtained by other techniques. (For details, readers are referred to the review articles cited in Further Reading and the original papers cited therein.)

SFG and SHG have been used for the study of adsorbates at surfaces even under ambient conditions. The adsorbate alters electronic or structural properties of the substrate and the signal is thus related to the surface density of the adsorbate and its orientation.

Elementary surface reactions, in particular adsorption, dissociation, or desorption of simple molecules such as CO, hydrogen, oxygen, or water on metal and semiconductor single-crystal surfaces under ultra-high-vacuum conditions, have been investigated. Sensitivity into the sub-percent monolayer regime is achieved and allows the identifictation of competing reaction channels and adsorbate dynamics on surfaces. Such studies can help to understand epitaxial growth or heterogeneous catalysis because the techniques are applicable at any gas pressure and surface temperature. Related to this is the study of surface diffusion, which can be probed following the temporal decay of a diffracted SHG signal off a submonolayer adsorbate grating formed by laser-induced desorption.

Making use of the spectroscopic capabilities of SHG, the surface electronic structure of selected metals and semiconductors, in particular silicon, were studied with an emphasis on the effects of temperature, crystallographic orientation and different adsorbates. Among buried interfaces, the Si/SiO_2 interface has been the subject of intense investigations and the sensitivity of SHG to static electric fields at the interface and to inhomogeneous strain was also demonstrated.

Different in-plane surface symmetries associated with different crystallographic orientations or surface reconstructions yield different SHG and SFG responses. This allowed for the investigation of surface reconstructions (e.g., $Si(111)2\times1 \rightarrow 7\times7$), order–disorder transitions (e.g., $Si(111)7\times7 \rightarrow 1\times1$, Au/Si(111)) and surface melting (e.g., single-crystal ice, Si(111), Ge(111)), providing information on latent heat, superheating, and its dynamics using pump-probe techniques. Magnetization-induced SHG was also used for probing surface and interface magnetism of ferromagnetic metals and bimetallic systems.

Many unique applications of spectroscopic SFG have been developed based on its capability to study large molecules, in particular under ambient conditions. Surface vibrational spectra with different input/output polarization combinations and sample geometries provide information on orientation, conformation and alignment of surface molecules and the composition and structure of the surface layer. The study of self-assembled monolayers (e.g., OTS on quartz) to deduce the orientation and conformation of the alkyl chains in the monolayer is an example. The effect of molecular density and temperature on the spectrum gives information on intermolecular interactions and phase transitions. Another example concerns the adsorption of liquid crystal molecules on nanostructured polymer substrates. Both the chain orientation at the polymer surface and its effect on the alignment of adsorbed liquid crystal molecules can be addressed.

Surface structures of liquids, especially those of pure liquids, are of great interest in science and technology, and SFG is a unique spectroscopic tool for probing liquid surfaces and interfaces. For example, the SFG vibrational spectrum for the water–vapor interface in **Figure 4** gives information on the density and orientation of the surface water molecules at the water–vapor interface. The surface layer was found to be more ordered compared to the bulk as was also observed for various other organic liquids studied with SFG. In other cases soluble and insoluble organic molecules at a liquid–vapor,

liquid–liquid, or liquid–solid interface have also been studied. They appear as adsorbed monolayer films and their structure and phase behavior are relevant to many applications. Identification of the adsorbed molecular species at solid–liquid interfaces is also important for understanding electrochemical processes. Various studies with SFG have addressed bonding of, e.g., CO, CN^-, and SCN^- at electrodes and its variation with electrode potential.

SFG spectroscopy also finds unique applications in studies of polymer surfaces and interfaces most relevant to modern science and technology. The observed surface vibrational spectra of polymers provide information on surface composition, molecular orientation, and conformation of neat and blended polymers. The effect of environment and surface treatment on the surface structure can also be studied. Investigation of the biological functions of complex molecular systems has attracted increasing interest, and SHG and SFG have been applied successfully to selected systems ranging from the isomerization of retinal – a molecule involved in the vision process – to functional aspects of model membranes.

Both SHG and SFG can be combined with microscopy techniques for surface microscopic studies. Microscopic imaging can be achieved by rastering the probe beam or, preferably, the sample position. Near-field SFG/SHG spectroscopy has recently been developed.

Performing surface SHG and SFG experiments in the time domain can provide information on surface dynamics. Pump-probe experiments allow for measurements of energy relaxation and phase coherence of excitations such as surface electronic states and surface phonons and vibrations.

Outlook

Although SHG and SFG were established as surface analytical tools more than 15 years ago, it is still an active field of research with much potential that has not yet been explored. As an example, it has only recently been demonstrated that doubly resonant infrared–visible SFG, as a two-dimensional spectroscopy, can give access to couplings between vibrational modes and surface electronic transitions. With the commercial availability of suitable laser sources, the techniques can be extended to a much wider range of applications. This includes possible investigations of ultrafast surface dynamics, nanostructures, and biological systems.

Further Reading

Bennemann KH (ed.) (1998) *Nonlinear Optics in Metals*. Oxford, UK: Clarendon Press.

Bloembergen N (1977) *Nonlinear Optics*. New York: Benjamin.

Boyd RW (1993) *Nonlinear Optics*, 2nd edn. San Diego, CA: Academic Press.

Dumas P, Weldon MK, Chabal YJ and Williams GP (1999) Molecules at surfaces and interfaces studied using vibrational spectroscopies and related techniques. *Surface Review & Letters* 6(2): 225–255.

Guyot-Sionnest P and Harris AL (1995) Surface vibrational dynamics probed by sum frequency generation. In: Ho W and Dai HL (eds) *Laser Spectroscopy and Photochemistry of Metal Surfaces*, pp. 405–458. Singapore: World Scientific.

Guyot-Sionnest P, Superfine R, Hunt JH and Shen YR (1988) Vibrational spectroscopy of a silane monolayer at air/solid and liquid/solid interfaces using sum-frequency generation. *Chemical Physics Letter* 144: 1–5.

Heinz TF (1991) Second-order nonlinear optical effects at surfaces and interfaces. In: Stegeman GI and Ponath H-E (eds), *Nonlinear Surface Electromagnetic Phenomena*, pp. 353–416. Amsterdam, The Netherlands: North-Holland.

Matthias E and Träger F (eds) (1999) *Applied Physics B, Special Issue: Nonlinear Optics at Interfaces*, Volume 210.

McGilp JF (1999) Optical second-harmonic generation as a semiconductor surface and interface probe. *Physica Status Solidi (a)* 175: 153–167.

Miranda PB and Shen YR (1999) Liquid interfaces: A study by sum-frequency vibrational spectroscopy. *Journal of Physical Chemistry B* 103: 3292–3307.

Reider GA and Heinz TF (1995) Second-order nonlinear optical effects at surfaces and interfaces: recent advances. In: Halevi P (ed.) *Photonic Probes of Interfaces*, 413. Amsterdam, The Netherlands: Elsevier.

Shen YR (1984) The Principles of Nonlinear Optics. New York: Wiley.

Shen YR (1994) Nonlinear optical studies of polymer interfaces. *International Journal of Nonlinear Optical Physics* 3: 459–468.

Shen YR (1994) Surface spectroscopy by nonlinear optics. In: Ḧansch TW and Inguscio M (eds) *Frontiers in Laser Spectroscopy*, pp. 139–165. Amsterdam, The Netherlands: North-Holland.

Shen YR (2001) Vibrational spectroscopy of water at interfaces. In: Morra M (ed.) *Water in Biomaterials Surface Science*, Chapter 8, pp. 215–244. Chichester, UK: Wiley.

Wei X and Shen YR (2001) Motional effect in surface sum-frequency vibrational spectroscopy. *Physical Review Letter* 86: 4799–4802.